Journal of Power Sources 248 (2014) 978–987

Contents lists available at ScienceDirect

Journal of Power Sources

journal homepage: www.elsevier.com/locate/jpowsour

A detailed thermal study of a $Li[Ni_{0.33}Co_{0.33}Mn_{0.33}]O_2/LiMn_2O_4$-based lithium ion cell by accelerating rate and differential scanning calorimetry

P. Röder [a,*], N. Baba [a], H.-D. Wiemhöfer [b]

[a] Robert Bosch GmbH, Corporate Sector Research and Advance Engineering, Robert-Bosch-Platz 1, 70049 Stuttgart, Germany
[b] Institute of Inorganic and Analytical Chemistry, University of Muenster, Corrensstr. 28/30, 48149 Münster, Germany

HIGHLIGHTS

- Performance of a thermal study of a lithium-ion battery (NCM/LMO vs. hard carbon).
- Thermal stability primarily depends on the positive electrode–electrolyte reaction.
- Inhibition of the oxidation reaction due to oxygen release can be seen in ARC studies.
- Completion of XRD studies and identification of several reduction products.
- Impact of the SOC studied by a combination of DSC and cyclic voltammetry (CV).

ARTICLE INFO

Article history:
Received 22 July 2013
Received in revised form
10 September 2013
Accepted 30 September 2013
Available online 17 October 2013

Keywords:
Lithium-ion
Safety
ARC
DSC
Cathode
NCM

ABSTRACT

Accelerating rate calorimetry (ARC) and differential scanning calorimetry (DSC) were used to study the thermal behaviour of a commercially available lithium-ion cell. Both the complete cell (pouch type, 2 Ah) and its electrode materials, respectively, were investigated. As positive electrode material a blend system consisting of NCM (=$Li[Ni_{0.33}Co_{0.33}Mn_{0.33}]O_2$) and LMO (=$LiMn_2O_4$) with a weight ratio of 4:1 was identified. The main exothermic behaviour is dominated by the positive electrode–electrolyte reaction. ARC studies on the positive electrode material in presence of our reference electrolyte show an inhibiting effect of the conducting salt $LiPF_6$ towards the oxidation of the organic based electrolyte by released oxygen. X-ray diffraction measurements were performed to study the thermal decomposition behaviour of the positive active material. Both the blend system and the single components, NCM and LMO, were investigated at different temperatures. A significant phase transformation from the hexagonal layered to a cubic structure as well as various reduction products could be identified. Finally, the thermal behaviour of the NCM/LMO-blend and its single phases, NCM and LMO, at different states of charge (SOC) was investigated. Therefore, detailed investigations based on differential scanning calorimetry (DSC) and cyclic voltammetry (CV) were performed.

1. Introduction

Lithium-ion cells have become promising power sources for portable applications and electric vehicles. Especially transition metal oxide based electrode materials, such as NCM (corresponding to $Li[Ni_{0.33}Co_{0.33}Mn_{0.33}]O_2$) or $LiCoO_2$ are used due to their good electrochemical performance and high capacity resulting in an acceptable high energy density [1,2]. Blend materials, commonly composed of spinel (e.g. $LiMn_2O_4$) mixed with a layered metal oxide are also commercially used [7,8]. However, concerns about the thermal behaviour of these oxide-based positive electrode materials still exist since oxygen release at higher temperatures can lead to a hazardous combustion reaction driving the flammable alkylcarbonate-based solvent of the electrolyte into fire or explosion. The thermal behaviour of complete lithium ion cells is primarily dominated by used electrode materials and their thermal decomposition behaviour as well as the reaction behaviour with the organic electrolyte [10–12]. Using C80 microcalorimetry, differential scanning calorimetry (DSC) or accelerating rate calorimetry (ARC), the thermal stability of several lithium-ion electrode materials in contact with salt-free solvent and electrolyte was already investigated by many researcher groups, e.g [3–6]. In this work, a detailed study of both the thermal behaviour of a complete

* Corresponding author. Tel.: +49 711 811 48718; fax: +49 711 811 5185972.
E-mail address: patrick.roeder@de.bosch.com (P. Röder).

0378-7753/$ – see front matter © 2013 Elsevier B.V. All rights reserved.
http://dx.doi.org/10.1016/j.jpowsour.2013.09.146

lithium ion cell and its electrode materials was performed by accelerating rate calorimetry (ARC) and differential scanning calorimetry (DSC), respectively. The active materials for the ARC experiments were obtained from the fully charged cell after disassembling in an argon filled glove box and afterwards rinsed with dimethyl carbonate (DMC). A similar study was already performed by Maleki et al. [9]. Maleki et al. investigated complete $LiCoO_2$-based prismatic lithium ion cells (550 mAh) by ARC and the respective electrode materials in contact with electrolyte by DSC. In our case the pouch type lithium ion cell from manufacturer A (see Table 1) contained a blend composed of $Li[Ni_{0.33}Co_{0.33}Mn_{0.33}]O_2$ (NCM) and $LiMn_2O_4$ (LMO) with a weight ratio of 4:1 (w/w) as positive electrode material. So called hard carbon was used as negative electrode material. We have investigated both the complete cell and its electrode materials by ARC experiments. The work of Maleki et al. as well as recent modelling works [13] have shown that especially the reaction between the positive electrode material and the organic electrolyte dominates the thermal reaction behaviour and leads finally to a thermal runaway.

Therefore, to understand the decomposition of the NCM/LMO-blend at elevated temperatures in detail, we have carried out X-ray diffraction measurements at different temperatures. Besides the blend material, the respective single phases NCM and LMO from commercially available lithium ion cells were also investigated by XRD. Moreover, we have analysed the impact of the conducting salt $LiPF_6$ towards the reaction behaviour between the positive electrode and a $LiPF_6$ based electrolyte by ARC. DSC was used to study the influence of the state of charge (SOC) towards the thermal behaviour of the NCM/LMO-blend in contact with the electrolyte. In this case, we have also carried out DSC investigations only on the single phases NCM and LMO, respectively, to understand the influence of the state of charge more precisely.

This work aims at a detailed study of the thermal safety behaviour of a complete lithium ion cell and the correlation to its electrode materials.

2. Experimental

2.1. Investigated materials

In all thermal and electrochemical experiments, a $LiPF_6$ based electrolyte consisting of a solution of 1 M $LiPF_6$ in ethylene carbonate (EC) and dimethyl carbonate (DMC) with a weight ratio of 1:1. This standard solvent mixture was commercially purchased.

Table 1 gives a short overview of the lithium ion cells and their electrode materials used for our ARC experiments. Therefore, we used three cell types from the respective manufacturer A, B, and C. In the following work, the cells will be indicated as cell A, B and C. The necessary chemical information are indicated in Table 1.

In the following, the abbreviation “NCM” always refers to the composition $Li[Ni_{0.33}Co_{0.33}Mn_{0.33}]O_2$ indicating the same ratio of nickel, cobalt and manganese. Several physical and electrochemical analyses (for instance XRD, etc.) were performed to determine and confirm the composition of the electrodes shown in Table 1.

Table 1
Overview of the lithium ion cells used for the thermal investigations.

Manufacturer [−]	A	B	C
Nominal Capacity [Ah]	2	2	1.2
Type [−]	Pouch	Pouch	Cylindric
Positive electrode [−]	NCM/LMO (4:1, w/w)	NCM[a]	LMO[b]
Negative electrode [−]	Hard Carbon	Graphite	Graphite

[a] NCM = $Li[Ni_{0.33}Co_{0.33}Mn_{0.33}]O_2$.
[b] LMO = $LiMn_2O_4$.

2.2. Thermal measurement method

2.2.1. Accelerating rate calorimetry (ARC)

To perform our ARC measurements the electrode materials were obtained from the respective commercially available lithium-ion cell from Table 1. Before disassembling, the cells had to be charged. The charge current I [A] is defined by the so called C-rate. Depending on the nominal capacity C_N [Ah] for each cell, shown in Table 1, the charge current is defined as followed (x [h^{-1}] as constant, e.g. 0.5 or 2): $I = x \cdot C_N$. Each cell was charged to 4.2 V with a defined charging rate of C/2 followed by a constant voltage step until the current dropped to a C/20 rate. Afterwards, the cell was discharged down to 2.5 V with the same current. This cycling procedure was repeated three times and ended with a final charging step up to a cut-off voltage of 4.2 V. The fully charged cell was then transferred into an argon-filled glove box and disassembled. The positive active material was scraped from the aluminium collector and rinsed with DMC to remove the original electrolyte and possible additives from the surface of the electrode material. Finally, the rinsed positive electrode material was dried under vacuum overnight to guarantee that all DMC was removed, before doing any ARC-experiments. The negative electrode material was not rinsed with DMC since organic components of the SEI could be removed by the rinsing procedure destroying the SEI [14,15].

The ARC samples, consisting of the prepared active material and the standard electrolyte (or salt-free solvent), were placed into a titanium sample holder with a wall thickness of only 0.1 mm. A sample mass of 200 mg of the cathode material and 100 mg (2:1 w/w) of the electrolyte were commonly used to carry out the ARC experiments. Due to the low density of the negative electrode material, in this case, only 100 mg of the negative electrode material and 50 mg electrolyte (2:1 w/w) were used. Since the electrode material was obtained from commercial lithium-ion cells, the weight of the electrode powder includes both conductive additives (crystalline and amorphous carbon) and binder. The whole sample preparation was made under argon atmosphere to prevent atmospheric influences (especially oxygen and water). All ARC experiments were carried out by an APTAC 254® (from Netzsch Gerätebau GmbH, Germany).

First of all, the samples were heated up to a start temperature of 80 °C. Commonly, a measurement stopped at 350 °C or when the self heating rate of the sample rised beyond 40 °C min^{-1}. In 5 K steps a heat-wait-search procedure (HWS) was applied with a waiting time of 15 min before searching for exothermal processes. If no exotherm was found, the temperature was increased with a heating rate of 5 °C min^{-1}. The threshold for an exothermic process was set to a heating rate of 0.02 °C min^{-1}. When the generated heat of our sample exceeded this threshold, the following exotherm was monitored under adiabatic conditions. Besides the detection of the temperature and the heating rate of our sample, we also recorded the pressure rise during an ARC measurement.

The ARC measurement of the complete lithium ion cell A, shown in Fig. 1, was performed at the Zentrum für Sonnenenergie- und Wasserstoff-Forschung in Ulm. The boundary conditions described above, such as heating rate or threshold for the detection of an exothermic process, were the same.

2.2.2. Differential scanning calorimetry (DSC)

Differential scanning calorimetry was used to investigate the influence of the state of charge (SOC) on the reaction behaviour between the positive electrode material and electrolyte. The NCM/LMO-blend based lithium-ion cell from manufacturer A was therefore charged to various SOC values (namely 100%, 80%, 60%,

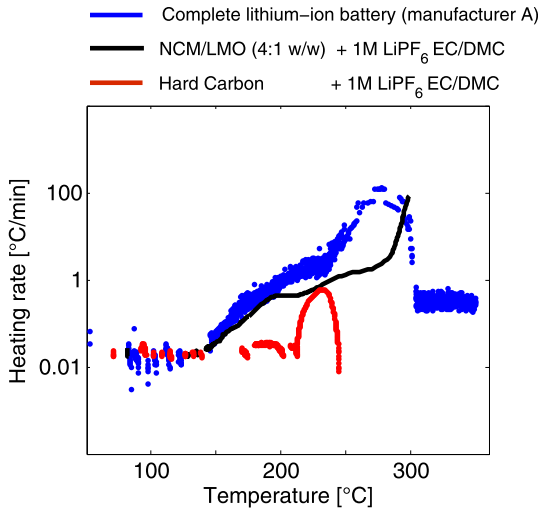

Fig. 1. Heating rate vs. temperature plot of the complete lithium ion cell (manufacturer A) and the respective electrode materials (200 mg) in contact with 100 mg electrolyte (1 M $LiPF_6$ EC/DMC (1:1, w/w)).

50%, 20%). The SOC was determined from the discharge capacity. To guarantee the same initial SOC for the single phases NCM and LMO (in-house prepared and coated), we determined the electrode potential of the positive blend electrode at the different state of charges within a potential test. Therefore, a test cell was built containing both the positive and negative electrodes from cell A. The test cell was equipped with a lithium reference, which was placed between the positive and negative electrode. Each of the various investigated states of charge correspond to a different electrode potential of the positive and negative electrode measured versus lithium. The test cell was cycled (1.614 mAh) with a rate of C/15. Afterwards, half cells containing the positive active material NCM or LMO versus lithium were built, respectively, and charged with a defined current to the electrode voltage determined by the test cell containing the electrode materials from cell A, as described. The in-house prepared NCM had a theoretical capacity of 157 mAh g^{-1} and the in - house prepared LMO of 105 mAh g^{-1}. The mass of NCM on the stamped blank for the half cell was 32 mg and for LMO 58 mg on the average. The area of the stamped blank was 2.54 cm^2. These values implied a capacity of 1.82 mAh cm^{-2} for NCM and 2.42 mAh cm^{-2} for the LMO cell, respectively. As cycling procedure for the half cells, two cycles with a C/15 rate were passed through before a final charging step occurred. After charging, the test cells were transferred into the argon filled glove box and afterwards disassembled. The active material was scrapped from the aluminium collector. The in-house coated NCM and LMO sheets were not calandered which made the removal of the active material much easier.

The DSC crucible contained commonly 12.5 mg positive active material. The DSC preparation was also done under argon atmosphere to prevent atmospheric influences. We used a scan rate of 5 K min^{-1} to carry out our DSC measurements. For every DSC measurement we built at least two half cells in order to check for reproducibility. For the thermal investigations it made no difference if the sheets were calandered or not. The positive electrode material was investigated in presence of our reference electrolyte. For the sake of comparability, we tried to adjust a mass ratio of 1:1 between the solid positive electrode material and the liquid electrolyte. The released heat as integral of the DSC plots was evaluated between 150 °C and 350 °C for all the DSC measurements.

2.3. Electrochemical and physical-analytical characterization methods

2.3.1. X-Ray diffraction (XRD)

In order to certify the crystalline structure of the delithiated positive electrode material and decomposition products at different temperatures, X-ray diffraction (XRD) measurements were carried out. The diffractograms were generated in an angle range between 5° and 100° (2θ) by a Bruker-AXS D8 diffractometer equipped with a Bragg-Brentano-optics. The 2θ angle in this paper correspond to the Cu-Kα radiation. XRD measurements were carried out on the positive electrode material. Therefore, we interrupted an ARC experiment at a defined temperature and performed XRD measurements afterwards. Since the complete ARC preparation occurs in the glove box, all the samples were heated up under argon atmosphere. XRD was also used to evaluate our rinsing procedure. To carry out the XRD investigations a so called scatter preparation was used. Therefore, the electrode powder was scattered on a specially cut quartz glass allowing no diffraction of the X-rays. The program TOPAZ (a software of Bruker AXS) was used to determine the crystalline structure and the corresponding lattice constants by a Rietveld refinement.

2.3.2. Cyclic voltammetry CV

Cyclic voltammetry (CV) was performed on the in-house prepared NCM and LMO sheets after punching versus lithium. Therefore a slow scan rate of 5 μV s^{-1} was used and three cycles were passed during the CV measurements.

3. Results and discussion

3.1. Thermal studies of the complete lithium ion cell and its positive electrode material studied by ARC

Fig. 1 shows the ARC measurements of the complete lithium ion cell from manufacturer A and its positive and negative electrode materials, respectively, in contact with 1 M $LiPF_6$ in EC/DMC (1:1, w/w). At this point, it should be mentioned that the original electrolyte of the complete lithium ion cell A is composed of 1 M $LiPF_6$ in a solution of ethylene carbonate and diethyl carbonate (DEC) (1:2, w/w). However, for the sake of comparability, we used for all our measurements our standard electrolyte with DMC instead of DEC as the difference in the linear carbonate should be negligible in our thermal analyses. In contrast to the measurement of the respective electrode materials in contact with the standard electrolyte the complete battery shows noisy data (black line). We ascribe this noisy behaviour to the measuring sensitivity of the thermocouple which is placed on the can surface of the complete battery during an ARC experiment. However, a clear course of the heating rate curve can be recognized, though a clear explanation for the noisy data stays unclear.

Between 80 °C and 120 °C the first small exothermic signals can be observed for the ARC measurement of the complete cell A. Our ARC measurements of the negative electrode material in contact with the standard electrolyte (red line) show exotherms in the same temperature range. The heating rates of these exotherms show no significant rise above the detection rate of 0.02 °C min^{-1}. In agreement with Maleki et al. [9], we ascribe these exotherms to the breakdown of the anodic SEI. Corresponding reactions at the negative electrode were already studied by many researcher groups [9,11,16]. In this study, the negative electrode reactions will not be further considered. At around 150 °C, we observe the start of a continuous rise of the heating rate of the complete lithium-ion cell reaching a maximum heating rate of 125 °C min^{-1}. Our measurement of the positive NCM/LMO-blend electrode in presence of

electrolyte (blue line) shows nearly the same onset-temperature and a comparable heating rate development. The deviation of the heating rate process of the complete lithium-ion cell around 200 °C can be ascribed to starting reactions at the negative electrode and the joule heat input by the internal short circuit occurring around 230 °C of the complete cell. The reaction of the negative electrode shows a maximum heating rate of nearly 1 °C min^{-1} (red line). We think that these exotherms correspond to the reactions between the intercalated lithium of the charged negative electrode and electrolyte [11]. Fig. 1 shows first and foremost that the thermal behaviour of the complete lithium-ion cell is primarily dominated by the reactions between the NCM/LMO blend (4:1, w/w) and electrolyte (black line). Hence, we have studied these reactions in detail.

Fig. 2 shows the pressure rise during an ARC experiment of the delithiated positive electrode material from the fully charged cell A (SOC 100%) without addition of electrolyte or solvent after the rinsing procedure as described in the Experimental section. Metal oxide based electrode materials decompose at higher temperatures. The decomposition is accompanied by oxygen release [3–6,17]. After reaching the shut down criteria of 350 °C, the experiment cools down to room temperature. The pressure rise is also recorded during cooling down to 50 °C. We denote the pressure at this point as irreversible pressure rise, in case of deviation from the initial pressure (usually 1 bar). Besides the active material, commercial positive electrode material compositions contain also binder material and conductive additives, such as crystalline or amorphous carbon. In case of cell A, graphite could be identified as conductive additive based on our XRD investigations with an amount of 2 wt.% (see Section 3.2). Although, the released oxygen can combust with these small amounts of graphite generating e.g. carbon dioxide, we assume that the irreversible pressure rise after cooling down is mainly generated by released oxygen during the thermal decomposition of the solid positive electrode material. Based on literature results [11] the binder should have no influence when the positive electrode material is investigated without addition of electrolyte or solvent.

The released oxygen can combust with the organic components of the electrolyte. Therefore, we tried to simulate this combustion reaction.

Fig. 3 (dashed line) shows the reaction behaviour of 200 mg delithiated positive electrode in contact with 60 mg of the corresponding salt-free solvent EC/DMC (w/w 1:1). In this case, the inorganic salt $LiPF_6$ was not present. At 150 °C a significant rise in

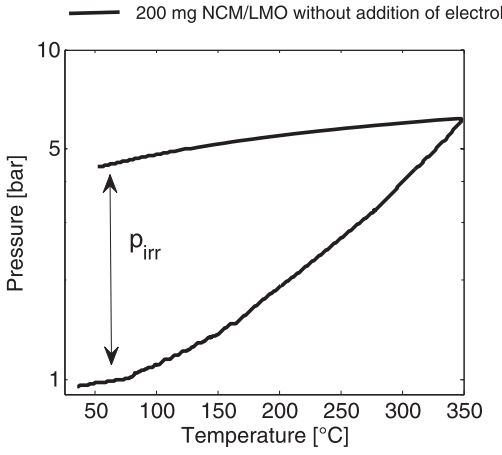

Fig. 2. Pressure vs. temperature plot of 200 mg delithiated NCM/LMO (4:1, w/w) blend (manufacturer A) without addition of electrolyte or solvent.

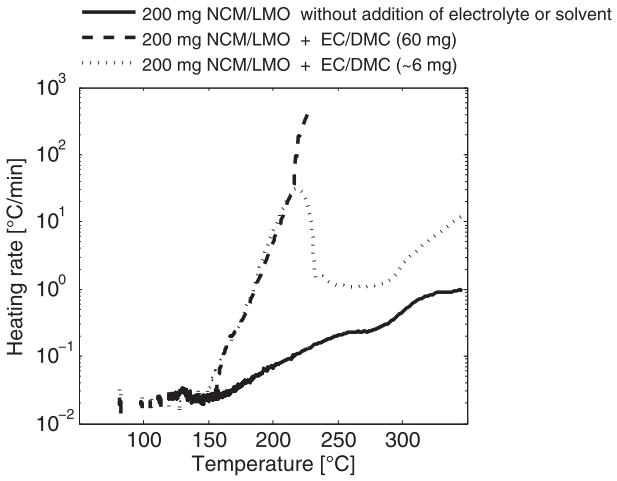

Fig. 3. Heating rate vs. temperature plot of 200 mg delithiated NCM/LMO (4:1, w/w) blend (manufacturer A) without addition of electrolyte or solvent (solid line) and in contact with 60 mg EC/DMC (1:1, w/w) (dashed line) as well as in contact with a calculated stoichiometric (spotted line) amount of EC/DMC (1:1, w/w).

the heating rate is observed. This onset-temperature is comparable with the measurement shown in Fig. 1. Hence, the reaction behaviour is primarily caused by the oxidation of the alkylcarbonate based solvent and released oxygen during the decomposition of the positive electrode material. In our case, the positive electrode of cell A is composed of NCM ($Li[Ni_{0.33}Co_{0.33}Mn_{0.33}]O_2$) and LMO ($LiMn_2O_4$) with a weight ratio of 4:1. Recent thermal investigations [1,17] on metal oxide based active materials (fully charged) have shown that the thermal decomposition occurs at different temperatures. The heating rate of the bare blend material without addition of electrolyte or solvent is also shown in Fig. 3 (solid line). Two significant exothermic processes with a plateau between 260 °C and 280 °C can be observed. We assume that each process results from oxygen release. Fig. In addition, 3 (spotted line) shows the thermal reaction behaviour of the electrode material in contact with a stoichiometric amount of EC/DMC (1:1, w/w) to simulate finally a nearly complete combustion reaction in our ARC according to:

$$C_3H_4O_3 + \frac{5}{2}O_2 \rightarrow 3CO_2 + 2H_2O \quad (1)$$

$$C_3H_6O_3 + 3O_2 \rightarrow 3CO_2 + 3H_2O. \quad (2)$$

To calculate the stoichiometric amount of EC/DMC (1:1, w/w) we used the irreversible pressure p_{irr} (=3.8 bar) of the bare blend material (200 mg) without addition of electrolyte or solvent shown in Fig. 2 after cooling down to 50 °C. As already mentioned, we make the simplification that this pressure rise is mainly generated by released oxygen. With the ideal gas equation (the volume V of the reaction room in our ARC was 1.5 cm^3) the molar amount of released oxygen $n_{O_2,\,released}$ could be calculated. Based on the stoichiometry Eqs. (1) and (2), the weight of the solvent EC/DMC (1:1, w/w) consumed due to oxidation by the available oxygen can be calculated according to Eq. (3):

$$m_{solv.,\,stoichio} = \frac{n_{O_2,\,released} \cdot M_{solv.}}{n_{O_2,\,solv.,\,stoichio}}. \quad (3)$$

$M_{solv.}$ (=89.1 g mol^{-1}) and $n_{O_2,solv.,stoichio}$ (=2.75 mol_{oxygen} $mol_{solv.}^{-1}$) are the calculated average values of the molar mass and the molar amount of oxygen consumed per mole EC/DMC (1:1, w/w) from Eqs. (1) and (2), respectively.

The stoichiometric measurement (spotted line) in Fig. 3 shows that two oxidation reactions occur with an onset-temperature of 150 °C and 280 °C, respectively. As suspected, both oxidation processes occur during the exothermic rise of the heating rate of the bare blend material without addition of electrolyte or solvent. It is evident that there is no increase in the heating rate for the measurement with the stoichiometric amount of EC/DMC (spotted line) in the temperature range between 260 °C and 280 °C. Simultaneously, no rise of the heating rate is observed in the same temperature range for the positive electrode material without addition of electrolyte or solvent (solid line).

At this point it should be mentioned that the decomposition of the solvent might not only be driven by the released oxygen. Especially the decomposition of the cyclic carbonate EC has to be taken into account.

Therefore, Fig. 4 shows the ARC (left) and DSC (right) result of 200 mg (ARC) and 10 mg (DSC) of the salt-free solvent EC/DMC (1:1, w/w). A continuous rise of the DSC curve can be observed with a maximum around 280 °C of nearly 0.2 W g^{-1}. The ARC measurement shows an onset temperature around 250 °C and a maximum heating rate of 0.15 °C min^{-1}. The onset temperature of the ARC measurement agrees well with literature data in which a thermal induced decomposition of EC is expected at 248 °C. A comparison of the ARC measurements shown in Fig. 3 (spotted and dashed line) and Fig. 4(a) by regarding the maximum heating rates and the onset-temperatures show that the reactivity of EC/DMC is significant lower when no electrode material is present indicating that oxygen release accompanied with an oxidation might be the driving force for the reaction behaviour when positive electrode material is present. Also the DSC measurement, in Fig. 4(b) shows a significant lower exothermic signal with 230 J g^{-1} compared to the reaction behaviour shown in Fig. 13 with a released heat of at least 650 J g^{-1}.

After these experiments, we have investigated the thermal reaction behaviour of the positive electrode material in contact with 100 mg of our reference electrolyte. In contrast to the measurements shown in Fig. 3 (dashed and spotted line), a salt concentration of 1 M $LiPF_6$ is now present.

The observed heating rate is shown in Fig. 5(a) (solid line). For comparison, Fig. 5(a) shows again the heating rate of the blend material in contact with a stoichiometric amount of EC/DMC (spotted line). It can be seen that the first exothermic process starting around 150 °C is significantly reduced when 1 M $LiPF_6$ is present by comparing the two measurements. However, the measurement of the blend material in contact with the $LiPF_6$-based electrolyte (solid line) shows a thermal runaway starting at around

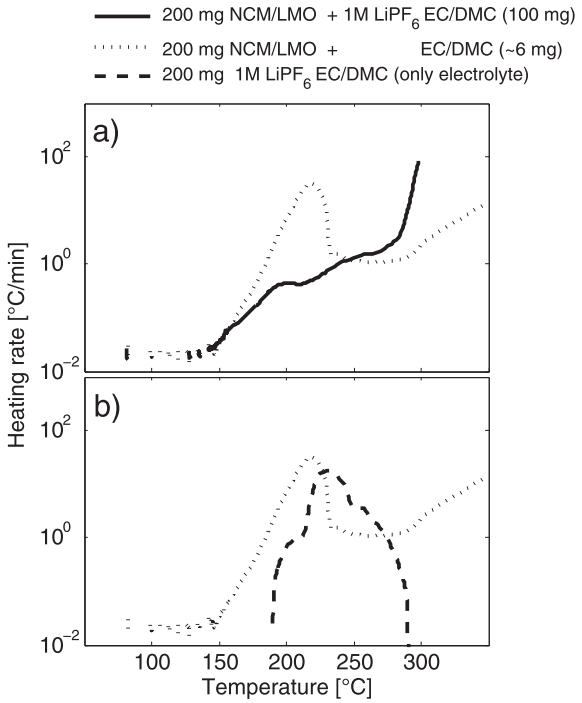

Fig. 5. (a): Heating rate vs. temperature plot of 200 mg NCM/LMO (4:1, w/w) blend (manufacturer A) in contact with 100 mg electrolyte (solid line) and in contact with a calculated stoichiometric amount of EC/DMC (1:1, w/w) (spotted line) and (b): in addition, the heating rate vs. temperature plot of 1 M $LiPF_6$ EC/DMC (1:1, w/w) without addition of electrolyte or solvent (dashed line).

280 °C according to a significant rise of the heating rate of the spotted line.

Fig 5(b) shows the heating rate of the reference $LiPF_6$ based electrolyte without addition of electrode material (dashed line) and again the heating rate of the blend material in contact with a stoichiometric amount of EC/DMC (spotted line). Both exothermic processes occur in the same temperature range. Detailed studies on our reference electrolyte were already described in a previous study [19] of us. The $LiPF_6$-based electrolyte shows an onset-temperature at 180 °C. We ascribe the first exothermic process of the electrolyte between 180 °C and 220 °C (dashed line) to the acid catalysed polymerization reaction of EC, as described by Sloop et al. [20] and Gnanaraj et al. [18]. Hereby, according to Eq. (5), the conducting salt $LiPF_6$ decomposes to LiF and the strong lewis-acid

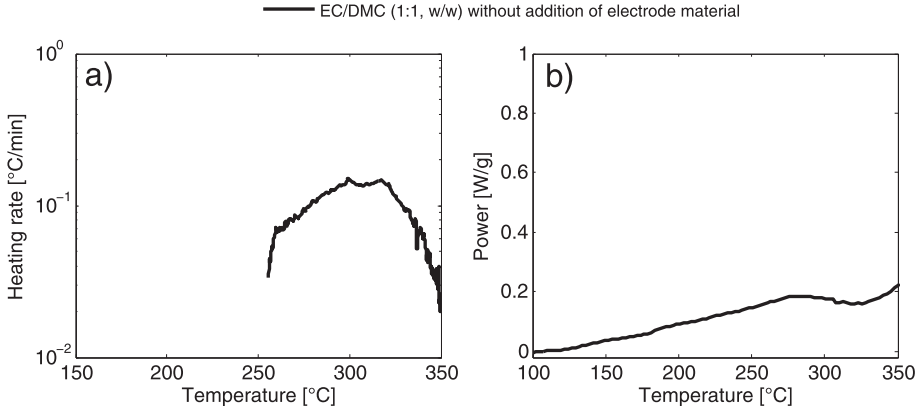

Fig. 4. (a) Heating rate vs. temperature plot (ARC) of 200 mg EC/DMC (1:1, w/w) without addition of solid electrode material and (b): corresponding DSC result of 10 mg EC/DMC (1:1, w/w) without addition of solid electrode material.

PF_5 inducing a ring opening of the cyclic carbonate EC. Impurity of water could also have an impact by generated HF according to Eq. (4).

$$PF_5 + H_2O \rightleftharpoons PF_3O + 2HF \quad (4)$$

As MacNeil et al. [26], we suspect that the PF_5 induced polymerization products inhibit the oxygen release causing the first exothermal oxidation process starting at 150 °C (spotted line). Besides that, a temporal delay of both the temperature and pressure progress can be observed in Fig. 6(a) and (b) when $LiPF_6$ is present. In this case, we used 60 mg of the reference electrolyte and the respective salt-free solvent for the sake of comparability.

3.2. Structural changes of the positive electrode material studied by XRD

Fig. 7 shows the XRD diffraction pattern of the NCM/LMO blend of cell A before and after rinsing with DMC, as described in the experimental section above. Table 2 shows the corresponding lattice constant of NCM and LMO. Within the measurement accuracy the lattice constants show no significant change. Based on error studies (here not shown), the fourth decimal place has to be neglected due to our preparation method and an error of +/− 0.001 nm must be considered. The XRD diffraction patterns in Fig. 7 are identical to the eye and, thus, the bulk structure of the positive electrode material was not changed during the rinsing procedure.

Primarily, XRD was applied to study the structural changes of the crystalline positive electrode material during thermal abuse. Fig. 8(a)–(c) shows the diffraction pattern of both the NCM/LMO blend from cell A and the respective diffraction patterns of the single phases NCM (manufacturer B) and LMO (manufacturer C) at room temperature. The electrode materials were obtained from the respective lithium ion cell shown in Table 1. The strongest diffraction lines of the layered structure of NCM (space group R3-m) and the cubic LMO structure (space group Fd3m) are indicated in Fig. 8(b) and (c), respectively. The same diffraction lines can be observed in the NCM/LMO blend material shown in Fig. 8(a). The intensity of the LMO diffraction lines are reduced due to its lower content in the respective NCM/LMO blend (4:1, w/w). In case of the NCM/LMO blend (cell A) and NCM from cell B an additional peak at

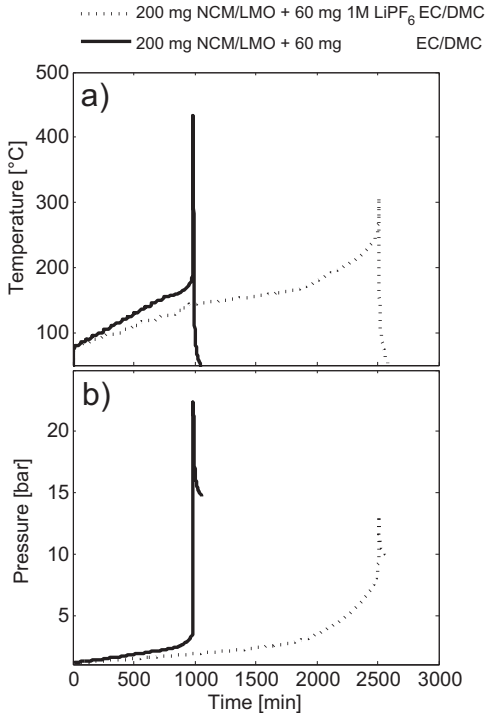

Fig. 6. (a): Temperature vs. time plot of 200 mg NCM/LMO (4:1, w/w) blend (manufacturer A) in contact with 60 mg electrolyte (1 M $LiPF_6$ EC/DMC (1:1, w/w)) (spotted line) and in contact with 60 mg salt-free solvent (EC/DMC (1:1, w/w)) (solid line) and b): corresponding pressure vs. time plot.

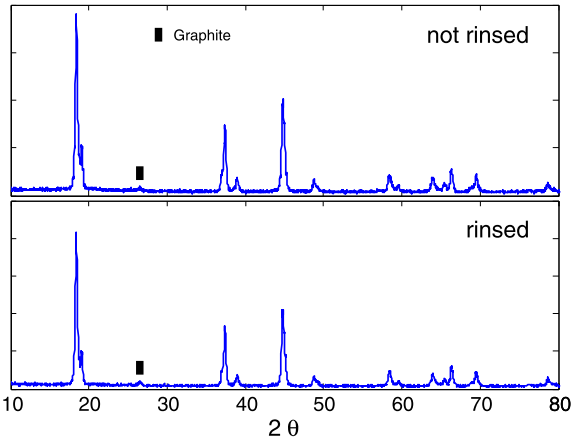

Fig. 7. XRD pattern of the delithiated NCM/LMO (4:1, w/w) blend (manufacturer A) without addition of electrolyte or solvent before and after the rinsing procedure at room temperature.

Table 2
Lattice constant of the delithiated NCM/LMO (4:1, w/w) blend (manufacturer A) before and after rinsing at room temperature.

–	a_{NCM} [nm]	c_{NCM} [nm]	a_{LMO} [nm]
Not rinsed	0.282(1)	1.452(3)	0.807(7)
Rinsed	0.282(0)	1.451(7)	0.807(3)

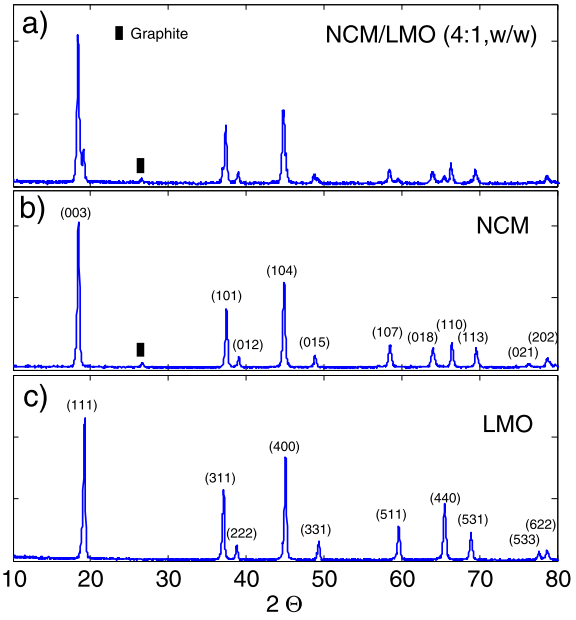

Fig. 8. (a): XRD pattern of 200 mg rinsed and delithiated NCM/LMO (4:1, w/w) blend (manufacturer A), (b): 200 mg delithiated NCM (manufacturer B) and (c): 200 mg delithiated LMO (manufacturer C) at room temperature, respectively.

26° can be observed. This reflex corresponds to graphite. Both graphite and amorphous carbon are used as conductive additives in the composition of the electrode material. We suspect that in case of LMO (Fig. 8(c)) amorphous carbon was used since no reflex at 26° could be identified. Our XRD studies could show that the amount of graphite in case of cell A and B is around 2 wt.% which is a typical quantity for conductive additives.

First of all, Table 3 shows the calculated lattice constants of the delithiated NCM/LMO blend without addition of electrolyte or solvent from cell A at room temperature and after an interrupted ARC experiment at 142 °C. In Fig. 3 (solid line) the heating rate of the delithiated bare blend material without addition of electrolyte or solvent shows an exothermic process between 120 °C and 140 °C with low heating rates around 0.02 °C min^{-1}. Since there is no significant change in the lattice constants, shown in Table 3, we can presume that there is no change of the bulk structure. After all, we can observe an exothermic process in this temperature range. Several publications [27–29] reported about protective layers formed on the positive electrode. We suspect thereby, that this exothermic process can be also related to an irreversible surface process. To confirm this assumption, we performed DSC measurements on the bare blend material from cell A. The results are shown in Fig. 9. Without opening the crucible, the delithiated blend materials were heated up three times after cooling down previously to room temperature. We could observe a reduction in the released energy after the second and third heating phase indicating that the exothermic process during the first heating phase is no more active. Further analytical studies on this effect have to be done, e.g. by XPS.

Fig. 10 shows the XRD diffraction patterns of the NCM/LMO blend at different temperatures. As described in Section 2 ARC measurements of the positive electrode materials in contact with our standard electrolyte were interrupted at the indicated temperatures shown in Fig. 10(a)–(d). Fist of all, at 210 °C a significant reduction of the LMO diffraction line at $2\theta = 19°$ is observed indicating a structural change of the LMO phase. With increasing temperature, a coalescence of the diffraction lines at 64° (NCM), 65° (LMO) and 66° (NCM) occurs resulting in a broad peak at 350 °C which indicates a new phase with a cubic structure. Nam et al. [24] studied already the structural change of NCM in contact with a $LiPF_6$ based electrolyte by time resolved XRD (TR-XRD) at different temperatures. In this study, a coalescence of the diffraction lines 64° and 66° corresponding to the NCM phase was observed. Nam et al. could verify a phase transition of NCM from the layered structure (R3-m) to a spinel like phase with a space group of Fd3m. With increasing temperature a rock salt phase with a space group of Fm3m was finally detected by Nam et al. We assume the same phase transition of the NCM in the NCM/LMO blend investigated in this study. To confirm this behaviour and especially to preclude the influence of the cubic phase LMO at 65°, the same study was made on the single phase NCM alone. Fig. 11(a)–(d) shows the resulting XRD patterns. As already expected, the same coalescence of the diffraction lines at 64° and 66° is observed. Since the diffraction lines are very broad, a Rietveld analysis would be quite complicated to determine the resulting phases at 350 °C. Assuming that the diffraction lines could be evaluated at higher temperatures, we heated the sample consisting of the NCM electrode powder and our electrolyte up to 490 °C. Therefore an ARC experiment was started under isothermal conditions. Since a thermal runaway occurs at around 280 °C (see Fig. 5(a)), we could not use a heat-wait-search modus generating adiabatic conditions as described in Section 2. Fig. 11(d) shows the resulting XRD pattern with sharp diffraction lines which could be

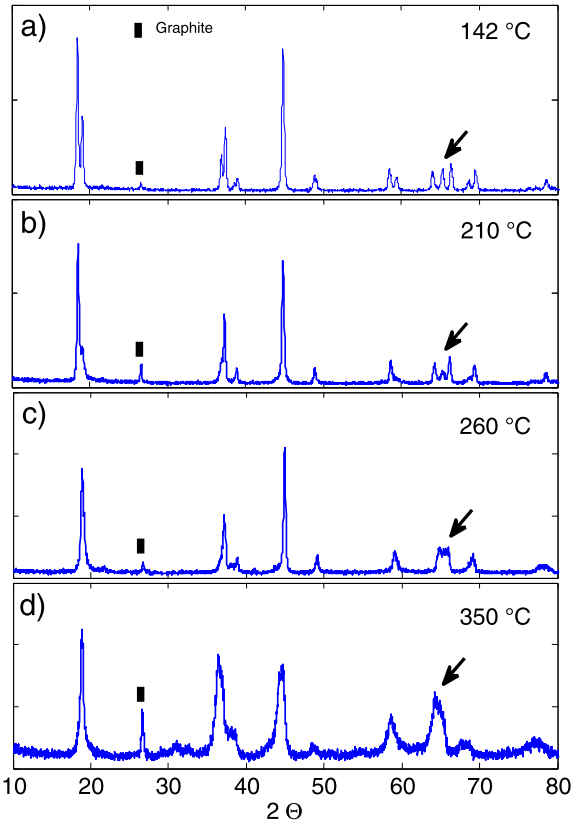

Fig. 10. XRD pattern of 200 mg delithiated NCM/LMO (4:1, w/w) blend (manufacturer A) in contact with 60 mg electrolyte detected after an interrupted ARC experiment at different temperatures.

Table 3
Lattice constant of the delithiated NCM/LMO (4:1, w/w) blend (manufacturer A) at room temperature and after an interrupted ARC experiment at 142 °C without addition of electrolyte or solvent.

-	a_{NCM} [nm]	c_{NCM} [nm]	a_{LMO} [nm]
Room temperature	0.282(0)	1.451(7)	0.807(3)
142 °C	0.282(0)	1.450(7)	0.807(4)

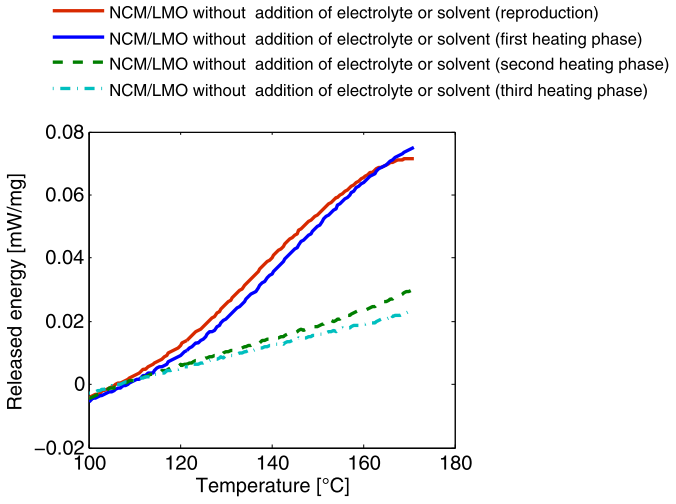

Fig. 9. DSC results of the delithiated NCM/LMO (4:1, w/w) blend (manufacturer A) without addition of electrolyte or solvent after three heating phases without opening the crucible.

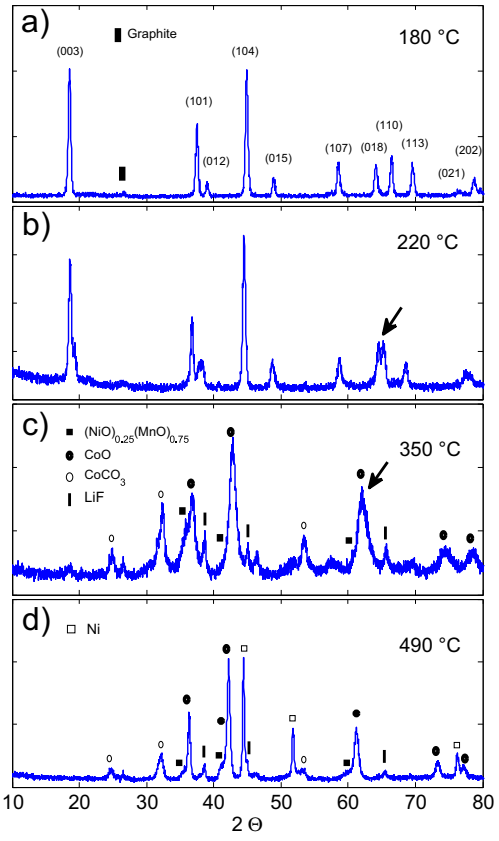

Fig. 11. XRD pattern of 200 mg delithiated NCM (manufacturer B) in contact with 60 mg electrolyte detected after an interrupted ARC experiment at different temperatures.

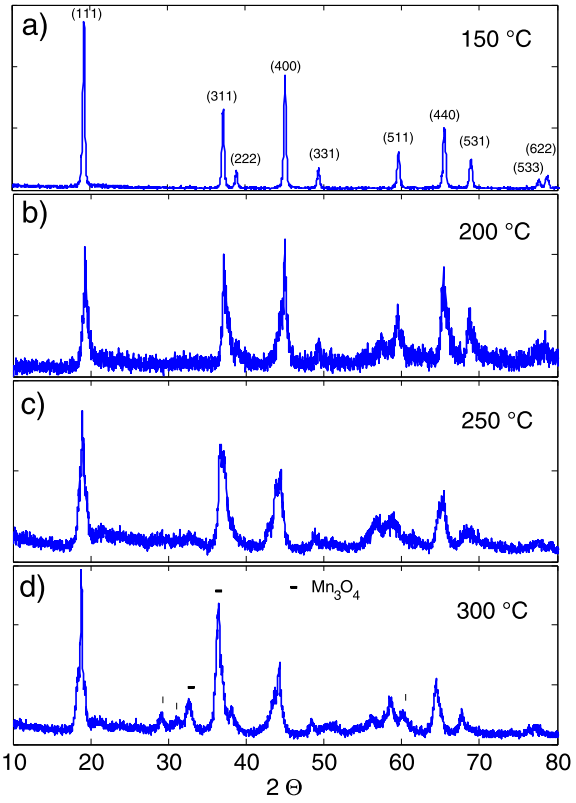

Fig. 12. XRD pattern of 200 mg delithiated LMO (manufacturer C) in contact with 60 mg electrolyte detected after an interrupted ARC experiment at different temperatures.

evaluated by a Rietveld analysis. In addition, the detected phases are shown in Fig. 11(c) and (d). In contrast to panel c), nickel was found as metallic phase. A (Mn,Ni)-oxide phase, i.e. $(NiO)_{0.25}(MnO)_{0.75}$, with the space group Fm3m could also be found. Both phases are reduction products accompanying the oxygen release. At higher temperatures (Fig. 11(c) and (d)) only a minor amount of NCM was still detected. Besides that, CoO, $CoCO_3$ and LiF were also observed. LiF is generated during the decomposition of the conducting salt $LiPF_6$ according to [20]:

$$LiPF_{6(s)} \rightleftharpoons LiF_{(s)} + PF_{5(g)} \quad (5)$$

MacNeil and Dahn [26] described the reaction of residual CoO with CO_2 to yield $CoCO_3$ during cooling down. CO_2 is generated during the combustion of the solvent EC/DMC (1:1, w/w) (Eqs. (1) and (2)) as well as during the polymerization of EC [18,20,26].

Finally, Fig. 12(a)–(d) shows the XRD patterns of LMO from cell C (see Table 1). In this case the reflections appear very broad making the evaluation quite difficult. However, the phase $Mn_3(II,III)O_4$ could be identified. This phase indicates also a reduction of the delithiated $Mn_2(IV)O_4$. MacNeil and Dahn [17] made similar thermal investigations with delithiated $LiMn_2O_4$ in contact with electrolyte. In this work Mn(II)O and $Mn_2(III)O_3$ were detected as reduction products in contrast to $Mn_3(II,III)O_4$. We assume that these reduction products are predominantly generated at higher temperatures. To confirm this assumption, the reaction products of LMO in contact with electrolyte have to be analysed, comparable to NCM, at higher temperatures. The corresponding studies will be done.

The XRD studies primarily show a phase transition of the layered electrode material NCM towards a crystalline structure with a space group Fm3m both in the blend system composed of NCM/LMO and in an electrode powder consisting only of NCM as active material. Moreover, the violent reduction of NCM in contact with electrolyte results in the generation of metallic nickel at higher temperatures. Based on these results, the following overall decomposition reaction can be assumed:

$$NCM(R3-m) \overset{\Delta T, solv.}{\rightarrow} (Mn,\ Ni)O(Fm3m) + CoO + Ni + O_2. \quad (6)$$

3.3. Impact of the state of charge (SOC) studied by DSC and CV

To investigate the influence of the state of charge (SOC), cell A was charged to different states of charge with subsequent disassembling to isolate the positive electrode material. In this case, the states of charge 20%, 30%, 50%, 60%, 80% and 100% were adjusted defined based on the discharge capacity of the lithium-ion cell as specified by the manufacturer A. Fig. 13(a) shows the DSC measurements of the NCM/LMO blend at different SOC's in contact with our standard electrolyte. First of all, a shift of the main exothermic peak around 300 °C towards lower temperatures can be observed with increasing SOC. At SOC = 50% and higher, an additional exothermic peak can be observed around 270 °C. Fig. 13(b) shows the resulting released heat as a function of the SOC. At SOC = 50% and higher, a significant increase in the released heat is observed accompanied by an additional exothermic peak, as already described.

To study this behaviour in detail, we have also investigated the single phases of the NCM/LMO blend. The experimental procedure is described in Section 2. Fig. 14(a) and (c) show the DSC plots of the single phases LMO and NCM at different voltages, respectively. These indicated voltages correspond to the electrode potentials of

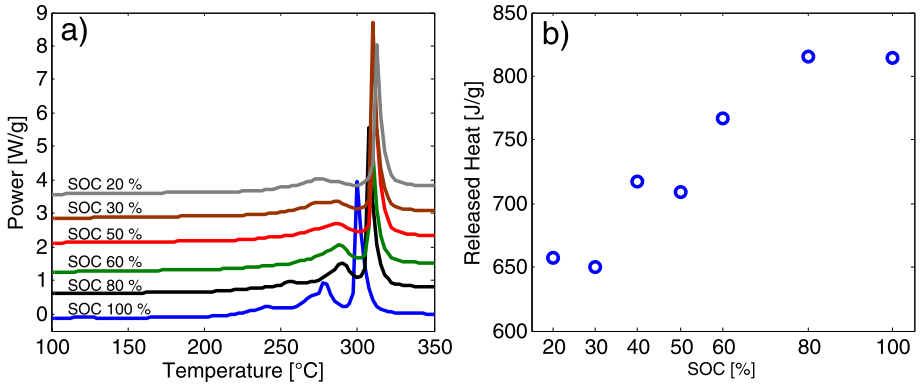

Fig. 13. (a): DSC results of the delithiated NCM/LMO (4:1, w/w) blend (manufacturer A) in contact with electrolyte at different state of charges and b): released heat at different state of charges of the delithiated NCM/LMO (4:1, w/w) blend (manufacturer A) in contact with electrolyte.

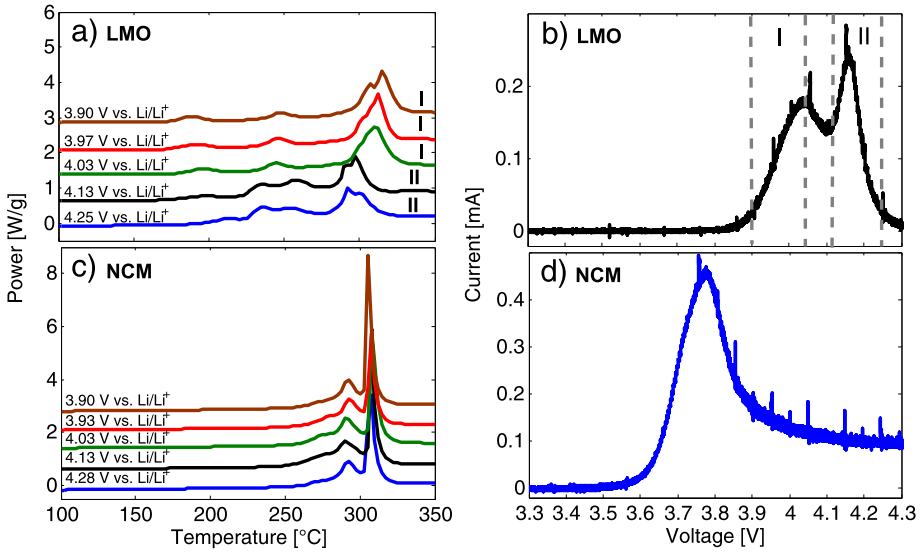

Fig. 14. (a) and (c): DSC results of the in house prepared NCM and LMO in contact with electrolyte at different voltages (vs. Li/Li^+), respectively, (b) and (d): cyclic voltammetry of the in house prepared NCM and LMO measured vs. Li/Li^+, respectively.

the positive NCM/LMO-blend material at different states of charge in cell A. In addition, the respective CV curves (Fig. 14(b) and (d) are shown. The CV curve of LMO shows two significant oxidation processes with maxima at 4.03 V and 4.15 V. This double-stage behaviour of LMO is well known [22,23] and corresponds to the stepwise increase of the average oxidation state of the Mn-ions from +3.5 ($LiMn_2O_4$) to +4 (λ-MnO_2) via an intermediate oxidation state of +3.75 ($LiMn_2O_4$/λ-MnO_2). In contrast, the CV curve of NCM shows only one significant process caused by the oxidation of Ni^{+2} to Ni^{+4} [21]. Corresponding to the CV plots, shown in Fig. 14(b) and (d), the respective delithiation mechanism of LMO and NCM can be described according to:

$$LiMn_2O_4 \rightarrow Li_{0.5}Mn_2O_4 \overset{II}{\rightarrow} Mn_2O_4(\lambda - MnO_2). \quad (7)$$

$$Li[Ni_{0.33}Co_{0.33}Mn_{0.33}]O_2 \rightarrow Li_{0.33}[Ni_{0.33}Co_{0.33}Mn_{0.33}]O_2. \quad (8)$$

Regarding the oxidation behaviour of LMO, two significant DSC characteristics (indicated with the roman numerals I and II in Fig. 14(a) can be observed. With the starting second oxidation process a shift of the exothermic DSC peak at around 300 °C towards lower temperatures and an additional DSC peak around 250 °C appears, which increases the released energy. The resulting DSC curves of NCM exhibit the same thermal characteristic for all electrode potentials. At 3.9 V, NCM has already passed the first oxidation progress, whereas LMO is still going to pass through both oxidation processes. We suspect thereby, corresponding to the oxidation behaviour of LMO, the second exothermic characteristic in the DSC curves observed at 4.13 V is related to a final increase of the oxidation state of the manganese ions to +4. As already suspected by Zhang et al. [6], the reaction and decomposition behaviour of metal oxide based electrode materials depend on the presence of transition metal ions with an oxidation state of M^{+4}. The final rise of the oxidation state of the manganese-ion to +4 significantly increases the released heat (see Fig. 15(a) and (b). Fig. 15(a) and (b) shows again the released heat of the NCM/LMO blend and in addition, the released heat of the single phases NCM and LMO, respectively, from Fig. 14(a) and (c). NCM shows a continuous rise of the released heat with increasing electrode potential corresponding to a higher SOC of cell A. As already suspected, LMO shows a significant increase of the released heat from 4.03 V to 4.13 V due to the final oxidation of the manganese ion to +4, as already described. The NCM/LMO blend shows also a significant rise of the released heat. We ascribed this rise of the released heat to the thermal behaviour of the LMO, described before. Nevertheless, NCM releases more heat as compared to LMO

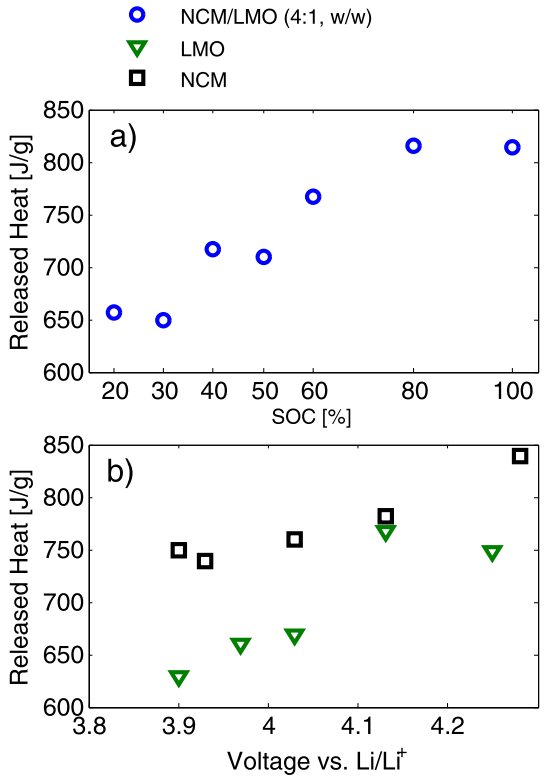

Fig. 15. (a): Released heat of the delithiated NCM/LMO (4:1, w/w) blend (manufacturer A) in contact with electrolyte at different state of charges, b): released heat of the delithiated and in house prepared NCM and LMO in contact with electrolyte at different voltages vs. Li/Li^+.

since the oxidation capability of Ni^{+4} [25] is stronger compared to Mn^{+4} leading to more oxygen release. We can conclude that a better understanding of the thermal reaction behaviour of the NCM/LMO blend (see Fig. 13(a) and (b) could be gained due to a combined study of both the electrochemical and thermal behaviour of the respective single phases NCM and LMO.

4. Conclusion

The ARC investigations in this work on the complete lithium-ion cell and its electrode materials, respectively, showed a significant dependence on the reaction behaviour of the positive electrode-electrolyte reaction. Both the heating rate progress and the onset-temperature of the positive electrode–electrolyte reaction agree well with the ARC-study of the complete lithium-ion cell (manufacturer A). Detailed thermal studies of the positive active material showed two significant oxidation reactions between the organic solvent and released oxygen, whereas the first oxidation around 150 °C is inhibited by the exothermal electrolyte decomposition reaction. XRD analysis both on the NCM/LMO blend material and the electrodes containing only NCM and LMO as active material showed a phase transformation of the layered NCM (R3-m) towards a cubic phase (Fm3m) which could be assigned to a (Mn,Ni)-oxide phase. Metallic Nickel could be identified at higher temperatures. Furthermore, thermal investigations based on DSC to study the impact of the state of charge on the reaction behaviour between the NCM/LMO blend and the $LiPF_6$-based electrolyte showed a significant rise of the released heat. Separate thermal-electrochemical studies on the single phases NCM and LMO by DSC and CV, respectively, showed that this energy input is generated due to the double-stage electrochemical oxidation behaviour of the manganese-ion to Mn^{+4}. However, the DSC investigations showed that the released heat of NCM in presence of electrolyte is higher compared to LMO during all states of charge related to the stronger oxidation capability of the Ni^{+4}-ion causing finally more oxygen release compared to the Mn^{+4}-ion.

Acknowledgements

We gratefully acknowledge the funding of this work within the Linacore and alpha-Laion Project by the Federal Ministry of Economy and Technology of Germany. The authors wish to thank the "Zentrum für Sonnenenergie-und Wasserstoff-Forschung" in Ulm for the ARC measurements of the complete lithium-ion cell and L. Epple (Robert Bosch GmbH) for the XRD analysis.

References

[1] I. Belharouak, Y.-K. Sun, J. Liu, K. Amine, J. Power Sources 123 (2003) 247–252.
[2] T. Ohzuku, R.J. Brodd, J. Power Sources 174 (2007) 449–456.
[3] Y. Wang, J. Jiang, J.R. Dahn, Electrochem. Commun. 9 (2007) 2534–2540.
[4] Q. Wang, P. Ping, J. Sun, C. Chen, Thermochim. Acta 517 (2011) 16–23.
[5] D.D. MacNeil, Z. Lu, Z. Chen, J.R. Dahn, J. Power Sources 108 (2002) 8–14.
[6] Z. Zhang, D. Fouchard, J.R. Rea, J. Power Sources 70 (1998) 16–20.
[7] H.Y. Tran, C. Täubert, M. Fleischhammer, P. Axmann, L. Küppers, M. Wohlfahrt-Mehrens, J. Power Sources 70 (1998) 16–20.
[8] T. Numata, C. Amemiya, T. Kumeuchi, M. Shirakata, M. Yonezawa, J. Electrochem. Soc. 158 (2011) A556–A561.
[9] H. Maleki, J.N. Howard, J. Power Sources 137 (2004) 117–127.
[10] S. Tobishima, K. Takei, Y. Sakurai, J. Yamaki, J. Power Sources 90 (2000) 188–195.
[11] R. Spotnitz, J. Franklin, J. Power Sources 113 (2003) 81–100.
[12] Q. Wang, P. Ping, X. Zhao, G. Chu, J. Sun, C. Chen, J. Power Sources 208 (2012) 210–224.
[13] H. Maleki, G. Deng, I.K. Haller, A. Anani, J.N. Howard, J. Electrochem. Soc. 174 (2000) A4470–A4475.
[14] Q.S. Wang, J.H. Sun, X.L. Yao, C.H. Chen, J. Electrochem. Soc. 153 (2006) A329–A333.
[15] E.P. Roth, D.H. Doughty, J. Franklin, J. Power Sources 134 (2004) 222–234.
[16] D.D. MacNeil, J. Electrochem. Soc. 146 (10) (1999) 3596.
[17] D.D. MacNeil, J.R. Dahn, J. Electrochem. Soc. 148 (11) (2001) A1211–A1215.
[18] J.S. Gnanaraj, E. Zinigrad, L. Asraf, H.E. Gottlieb, M. Sprecher, D. Aurbach, M. Schmidt, J. Power Sources 119–121 (2003) 794–798.
[19] P. Röder, N. Baba, H.-D. Wiemhöfer, J. Power Sources 236 (2013) 151–157.
[20] S.E. Sloop, J.B. Kerr, K. Kinoshita, J. Power Sources 119–121 (2003) 330–337.
[21] H. Kobayash, Y. Arachi, S. Emurac, H. Kageyama, K. Tatsumi, T. Kamiyamad, J. Power Sources 146 (2005) 640–644.
[22] M. Winter, J.O. Besenhard, M.E. Spahr, P. Novak, Adv. Mater. 10 (1998) 744–745.
[23] G.G. Amatucci, C.N. Schmutz, A. Blyr, C. Sigal, A.S. Gozdz, D. Larcher, J.M. Tarascon, J. Power Sources 69 (1997) 11–25.
[24] K.-W. Nam, W.-S. Yoon, X.-Q. Yang, J. Power Sources 189 (2009) 515–518.
[25] H. Konishi, T. Yuasa, M. Yoshikawa, J. Power Sources 196 (2011) 6884–6888.
[26] D.D. MacNeil, J.R. Dahn, J. Electrochem. Soc. 149 (7) (2002) A912–A919.
[27] A. Veluchamy, C.-H. Doh, D.-H. Kim, J.-H. Lee, H.-M. Shin, B.-S. Jin, H.-S. Kim, S.-I. Moon, J. Power Sources 189 (2009) 855–858.
[28] M. Xu, W. Li, B.L. Lucht, J. Power Sources 193 (2009) 804–809.
[29] R. Dedryvère, H. Martinez, S. Leroy, D. Lemordant, F. Bonhomme, P. Biensan, D. Gonbeau, J. Power Sources 174 (2007) 462–468.